J Forensic Sci, November 2008, Vol. 53, No. 6
doi: 10.1111/j.1556-4029.2008.00876.x
Available online at: www.blackwell-synergy.com

David J. Daegling,[1] *Ph.D.; Michael W. Warren,*[1] *Ph.D.; Jennifer L. Hotzman,*[1] *M.A.; and Casey J. Self,*[1] *M.A.*

Structural Analysis of Human Rib Fracture and Implications for Forensic Interpretation*

ABSTRACT: Patterns of rib fractures are of significant clinical and forensic interest. Linking patterns of rib fracture with specific physical events provides a foundation for understanding the nature of traumatic events that are associated with rib fracture in forensic contexts. In this study, isolated human ribs (n = 8) were end-loaded to failure to investigate: (i) local deformations (bone strain) prior to and during structural failure, (ii) location of ultimate failure, and (iii) fracture mode. Structural properties of ribs were used to calculate theoretical stresses to determine whether such calculations could be used to predict site of fracture. Ribs fractured on the sternal side of midshaft in all experiments, but mode of failure varied with transverse, buckle, spiral, and "butterfly" fractures observed. Comparison of calculated stress with observed strain values suggest that experimental, rather than theoretical, approaches will be most productive in furthering understanding rib fracture in forensic contexts.

KEYWORDS: forensic science, forensic anthropology, bone biomechanics, stress, strain, skeletal trauma

Rib fractures are commonly associated with traumatic events in clinical and forensic contexts, yet the etiology of rib fractures with respect to traumatic loads is poorly understood. If forensic anthropologists are to make contributory statements as to the mechanism of thoracic injury as it relates to cause and manner of death, further research is required to better understand the biomechanics, structure, and composition of ribs. Empirical demonstration of variability of rib fracture patterns with respect to loading conditions advances this understanding.

Love et al. (1,2) comprehensively outlined the difficulties involved in relating rib fractures to the mechanical circumstances that cause them. They presented a classificatory system for characterizing fracture patterns and noted that simple consideration of bone's material behavior was insufficient for understanding the variety of fracture patterns seen in blunt force trauma victims. This paper follows their recommendation for further research; specifically, we present experimental evidence on the structural behavior of ribs under controlled loads in an attempt to identify those mechanical variables that permit prediction of fracture mode and location in human specimens. Such data are potentially valuable for reconstructing the circumstances accounting for rib fractures in forensic contexts.

Love and Symes (2) observed multiple examples of adult rib fractures in which there is evidence of initial failure in compression and incompleteness of fracture. They interpreted these findings as being "contrary to current biomechanical principles of elastic bone" (2, p. 1153). Their rationale was that: (i) bone as a tissue is relatively weak in tension, and therefore should preferentially fracture in that mode and (ii) mature bone is relatively stiff, and this should predispose adults to brittle fractures that will be catastrophic and complete. If the structural properties of whole ribs are considered in conjunction with material considerations, observations of incomplete and compressive rib fractures are explicable in biomechanical terms.

Fracture in bone can be studied from material or structural perspectives. Conceptualizing bone as a *material* essentially considers analysis at the tissue level; material variables include elastic modulus (stiffness) and toughness (resistance to fracture), among others. Elastic modulus is the ratio of stress to strain within the functional range of loading; stress is reckoned as force per unit area (N/mm^2 or the MegaPascal [MPa]) while strain is a measure of the deformation associated with stress and is calculated as the change in length under load relative to original length, and is therefore dimensionless. Materials with high modulus values are said to be *stiff*, those with low values are called *compliant*. Toughness, in the vernacular, measures a material's ability to resist cracking; in the biomechanical context it is measured in terms of energy absorption or *work of fracture* (3) and is figured in units of Joules per square meter (J/m^2).

The structural perspective in the osteological context is concerned with whole bone behavior. Considerations of size and shape become important, because the behavior of the whole bone is dependent on details of cross-sectional geometry and local and regional variations in cortical bone thickness. Structural variables of interest include *second moments of area* (I), which account for the area of stress-resisting material and its distribution in a cross-section of interest. These variables permit calculation of structural stiffness and strength that are important for understanding how whole bones fail.

In mechanical terms, bone *strength* can have different meanings. Structural strength refers to the load at which a particular specimen fails. By this concept a femur is stronger than a metacarpal, and simply reflects the fact that femora are larger and more massive than hand bones. Material strength refers to the stress at which failure occurs. If bone tissue was universally invariant in its composition, it would fail at the same stress, whether failure of a rib, humerus, or parietal was considered. Material strength is potentially useful for modeling bone failure because if it can be established that bone tissue in a particular skeletal element exhibits a restricted range of material property

[1]Department of Anthropology, University of Florida, 1112 Turlington Hall, Gainesville, FL 32611-7305.

*Presented at the 58th Annual Meeting of the American Academy of Forensic Sciences in Seattle, WA, February 20–25, 2006.

Received 18 Sept. 2007; and in revised form 16 Mar. 2008; accepted 19 Apr. 2008.

variation, it may be possible to specify a narrow range of stress over which failure is likely to occur.

With respect to bone, strength can be further partitioned in terms of *yield strength* (or stress) and *ultimate strength* (or stress). While ultimate strength refers to the stress at which bone tissue actually fractures macroscopically, yield strength is the stress at (and beyond) which bone undergoes permanent plastic deformation (i.e., the original shape is irrecoverable). In the forensic context, ultimate strength is presumably the stress measure of interest.

Predicting bone fracture is theoretically straightforward if knowledge of loading conditions and a complete accounting of material and structural composition are known *a priori*. As this information is rarely accessible even in the context of laboratory testing, models of bone fracture are necessarily grounded in an experimental foundation (4,5). The difficulty in forensic contexts is that trauma is seldom comparable among cases; thus, in *post hoc* comparisons, it is not surprising that rib fracture patterns are inconsistent (1). What remains to be established however, is whether morphological variation alone is sufficient to present an array of fracture types and locations.

The experiments described below were performed to address the following questions: (i) when loads are controlled, is fracture mode and location among a sample of ribs consistent? and (ii) is the variation in fracture pattern explicable with reference to structural variables that consider variation in biomechanical performance among different specimens? The first question asks whether a defined traumatic event can be expected to yield a signature fracture, while the second question asks whether there are feasible computational biomechanical approaches that can be easily applied to predict and understand variability in rib fracture patterns.

Methods

Eight ribs were subjected to end-compressive loading until failure. During load application, surface bone strain was recorded from four locations on the ribs. From the strain data, estimates of local stress were calculated for purposes of assessing local liability to fracture. Location and mode of fracture was noted for each specimen. Details and rationale for the above procedures follow.

Ribs (n = 8) were obtained from existing research and teaching collections at the University of Florida (Institutional Review Board UF granted exempt status to this protocol). Sex and age data were not available for the sample, but all represent adult individuals. The particular ribs represented are unknown in each case; however, the elements represented are from ribs 3 to 9 based on morphological criteria (6). Specimens 1 and 3 were antimeres of one individual. Because specimens were dry and degreased, prior to mechanical testing specimens were rehydrated in saline for 24 h prior to testing in order to more closely recover *in vivo* structural behavior (4). Drying of bone results in an increase in both elastic modulus and strength from values derived for fresh bone (7), but rehydration of dry specimens in saline restores the wet weight, stiffness, and work of fracture to presumed *in vivo* levels (8,9). For this reason, rehydration is routinely practiced in bone mechanical testing (10) and is recommended to best approximate *in vivo* behavior (11). Evidence that physiological bending strength may not be fully recovered by this procedure (9) is not detrimental to the present study, as our focus is on the predictability of fracture mode and location rather than the determination of structural strength.

To measure surface deformation in specimens, 3-element rosette strain gages (FRA-1-1 L; Texas Measurements, College Station, TX) were bonded to each specimen. Gages were applied on superficial (parietal) and deep (visceral) surfaces at the angle, and on the corresponding surfaces of the sternal shaft, midway between midshaft and the sternal end. Strains were continuously recorded during experiments at 100 samples/sec. From the recorded strains the maximum principal strain (ϵ_1), minimum principal strain (ϵ_2), and shear strain (γ) were determined, as was the orientation of ϵ_1.

The head and neck and sternal ends of the ribs were embedded in a thick sleeve of vinyl polysiloxane putty (3M Dental Products, St. Paul, MN) to mitigate potential stress concentrations at the sites of restraint and load application. Both sleeves were fitted to hard rubber bumpers, which were secured to the load actuator (head end) and the platen (sternal end). The load was applied perpendicular to the head-tubercle axis in order to apply a bending moment to the specimen (Fig. 1). While this procedure cannot be expected to mimic the *in vivo* context precisely, it was intended to simulate anteroposterior compression of the thorax by producing tension along the convex parietal surface and compression along the visceral concave surface. The load was applied at a rate of 0.5 mm/sec until structural failure was observed.

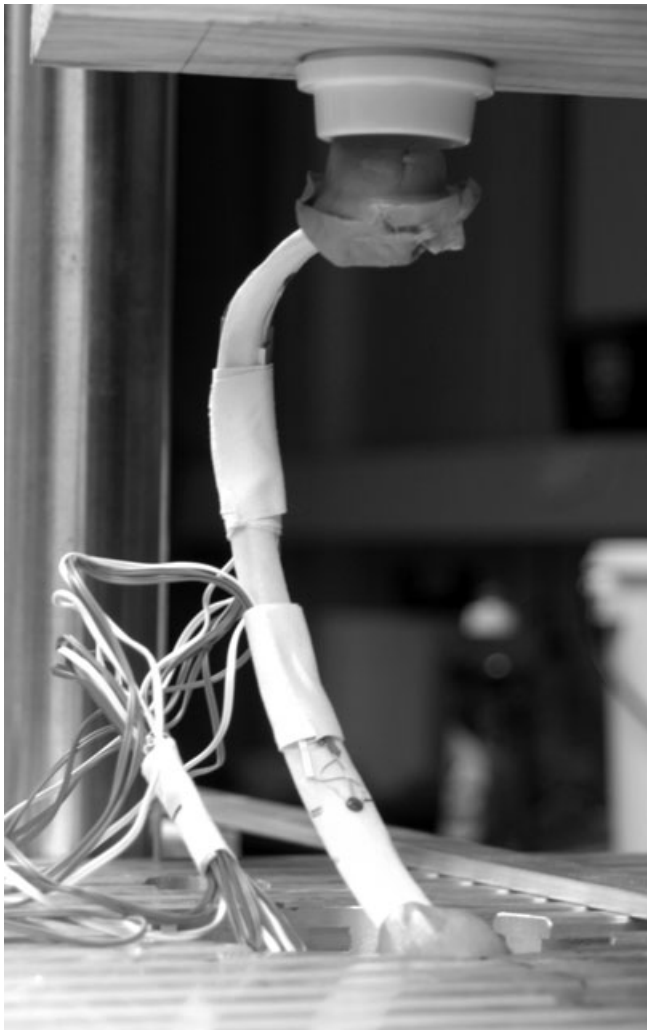

FIG. 1—*Experimental specimen prior to loading. The vinyl putty sleeves at each end served to minimize stress concentrations at the site of load application (top) and restraint (bottom). Each specimen was instrumented with four strain gages. The end load applied created a bending moment which placed the outer surface of the rib in tension and the inner surface in compression. Load was applied at a constant rate of 0.5 mm/sec until failure.*

Following experiments the structural properties of the ribs were estimated from external measurements of thickness and depth. The bending stiffness of the angle, midshaft, and sternal portions of the ribs was calculated based on an assumption of elliptical geometry (12). A theoretical stress at these locations was then calculated using existing elastic modulus data on human ribs (13). At locations of strain gage attachment, an "observed" stress was also calculated under the same assumption of elasticity. Idealizing a rib as a prismatic, uniformly curved structure that is end-loaded in the manner of our experimental procedure, the expectation is that—given minor variation in material and structural properties throughout the element—failure is likeliest at midshaft.

In general terms, the location of the greatest structural weakness will correspond to the presentation of a fracture. Yet the location of the highest principal stress may or may not represent the ultimate site of failure. The production of a fracture is closely tied to the release of strain energy (5), and shear stress and strain are also implicated in bone failure (14). Which stress or strain variable is best recruited for understanding bone failure is context-dependent and remains an area of ongoing experimental investigation (15). As both principal and shear stresses and strain energy will be proportional to principal and shear strains, the strain gage data can nevertheless be utilized to assess where regions of structural weakness may be encountered.

The manner of specimen loading was intended to induce bending coincident with the rib's longitudinal axis. Given the force applied, the magnitude of the bending moment can be calculated for any section of the rib, which for this study included strain gage locations and the eventual site of fracture. These data, when related to the stiffness measures calculated for rib sections, could then be used to model relative stresses along the rib shaft, with the expectation that the location of the highest calculated stresses would correlate with sites of failure.

Calculation of stress under bending loads involves the common flexural formula, or $\sigma = Mc/I$, where σ is the stress, M is the magnitude of the bending moment, which is the product of the applied force and its moment arm (a linear measure analogous to leverage), c is the distance of the locality of interest from the bending neutral axis, and I is the appropriate second moment of area. The equation assumes that the structure in question is geometrically, structurally, and materially invariant throughout, which of course is unrealistic to some degree for bone. Still, this approach is used widely within anthropology to draw functional inferences concerning skeletal variation (16).

Fracture location was described both categorically and quantitatively. Measuring the arc of the parietal surface of the rib, each specimen was divided into quartiles based on the cumulative proportion of the arc, as measured from the head end: 0–25%, head end; 25–50%, angle midshaft; 50–75%, sternal midshaft; 75–100%, sternal end. In addition, the exact location of the fracture was noted as a percentage of the total arc from the head end. Assessment of fracture mode included whether the fracture was complete or incomplete and otherwise categorized as buckle (incomplete by definition), transverse, spiral, or butterfly (Fig. 2).

Results

One specimen (no. 2) failed immediately upon restraint via a buckle fracture along the sternal portion of the shaft. This failure occurred as the result of longitudinal compression as it presented on the visceral surface. No strain data or theoretical stresses were collected on this specimen.

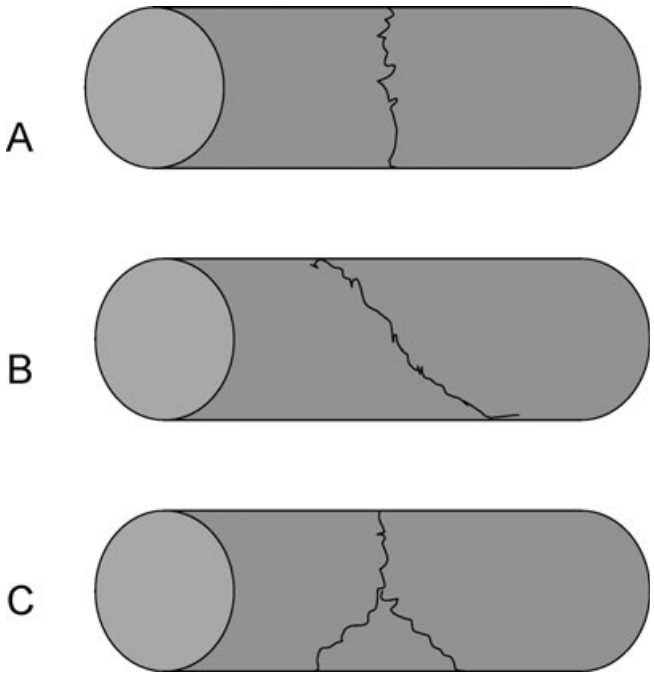

FIG. 2—*Schematic representation of fracture modes. (A) transverse fractures are defined as running perpendicular to the bone long axis. (B) spiral fractures follow a sigmoid pattern. (C) "Butterfly" fractures are typified by a transverse portion that terminates as two obliquely disposed lines of failure. These categories are idealized and modes of fracture in bone are considerably more varied than implied by these distinctions. See text for mechanical explanation of these fracture modes.*

The above specimen excepted, fracture location was very consistent (Table 1), with all specimens fracturing in the sternal midshaft region. In this region the cross-sectional shape of the ribs is eccentric, with the superior inferior dimension far exceeding the mediolateral dimension. Under the imposed loads, the ribs are predisposed to initial failure along the parietal or visceral surfaces.

Fracture mode was variable (Table 1). Four experiments terminated with incomplete fractures. These included the one buckle fracture noted above, as well as three of four transverse fractures. In one specimen (no. 3), the fracture initiated transversely on the parietal surface (i.e., under longitudinal tension), but terminated as a complete spiral fracture on the visceral face. Other complete fractures included specimens exhibiting butterfly and spiral patterns.

The theoretical stresses at gage locations and at the sites of fracture indicate relatively low stresses at the rib angle and typically larger stresses at fracture sites and the sternal region of the shaft (Table 2). In three cases, the calculated stresses suggest that failure

TABLE 1—*Observed fracture patterns.*

Specimen	Fracture Location (% from head)	Fracture Type	Fracture Severity
1	sternal midshaft (60.9)	transverse	complete
2	sternal midshaft (74.2)	buckle	incomplete
3	sternal midshaft (60.0)	transverse+spiral*	complete
4	sternal midshaft (62.1)	butterfly	complete
5	sternal midshaft (53.4)	spiral	complete
6	sternal midshaft (61.0)	transverse	incomplete
7	sternal midshaft (67.1)	transverse	incomplete
8	sternal midshaft (64.8)	transverse	incomplete

*fracture initiated on parietal surface in tension as a transverse fracture and terminated as a spiral fracture on the visceral surface.

TABLE 2—*Theoretical stress magnitudes.*

Specimen	Breaking Stress	Shaft Stress	Angle Stress
1	78.5	20.9	49.3
3	92.2	72.6	30.1
4	93.5	54.7	11.1
5	48.6	48.2	38.0
6	32.7	37.0	8.8
7	64.2	84.1	22.6
8	149.7	94.3	54.6

Units in MPa. Stresses were calculated based on the common flexural formula (see text), and are based on the load at failure. Shaft and angle stresses are calculated at respective strain gage sites. Breaking stress is estimated at the site of failure. All calculations assume that the ribs are solid structures.

should have occurred in the vicinity of the strain gages on the sternal portion of the shaft. The general prediction that—given the load conditions, rib curvature, and rib shaft dimensions—failure would occur in the vicinity of midshaft is borne out in the remaining specimens. In all but one case (specimen 8), a reasonably precise (*c.* 5 mm) fit of predicted versus actual site of fracture was observed.

With the exception of specimen 1, the theoretical stress values suggest that the measured strains should be between about 1.3 and nearly five times larger at the sternal shaft gages in comparison with the gages located at the angle (Table 2). In fact, the outer sternal shaft tensile strains (ϵ_1) are universally larger than the outer angle strains by factors ranging from 1.2 to 13.5, and on inner surfaces the ratio of shaft to angle compressive strain (ϵ_2) ranges from 1 to 9.8 (Table 3). Thus, there is substantial disparity between relative theoretical stress magnitudes and observed strain magnitudes.

Under the load case applied, it is also expected that the ratio of maximum to minimum principal strain (ϵ_1/ϵ_2) will be greater than unity on parietal surfaces and below unity on visceral surfaces. This is observed across all specimens, despite a large amount of inter-individual variation. The direction of maximum principal strain was similarly variable across the sample (Fig. 3), although the overall distribution of these orientations is consistent with what is expected from a bending load of the type applied. There are several observations of very large strains along the sternal shaft, including one case (specimen 8) in which tensile strains on the outer shaft exceed published yield strain values for bone (5). In addition, nonlinear changes in load with increasing displacement were observed prior to failure in several ribs (specimens 3, 4, 5, 8). This, in addition to the observation of large strains noted above, suggests plastic deformation of specimens was occurring well before local fracture was observed and experiments terminated.

TABLE 3—*Strains at failure.*

Specimen	ϵ_1 ($\mu\epsilon$)	ϵ_2	γ	angle ϵ_1	ϵ_1/ϵ_2	Yield Load (N)
Outer Angle						
1	2735	−803	3538	34.3	−3.406	−85.06
3	2331	−1074	3405	72.5	−2.170	−92.47
4	707	−378	1085	53.1	−1.870	−37.73
5	4384	−1743	6127	38.1	−2.515	−47.06
6	638	−345	983	42	−1.849	−19.14
7	1500	−453	1953	33.8	−3.311	−29.20
8	3436	−1350	4786	39.2	−2.545	−65.92
Inner Angle						
1	−2250	−2330	80	−86.4	0.966	−85.06
3	1108	−3461	4569	8.8	−0.320	−92.47
4	866	−1391	2257	−61.2	−0.623	−37.73
5	1988	−4352	6340	−44.3	−0.457	−47.06
6	98	−543	641	−62.9	−0.180	−19.14
7	277	−1395	1672	−21.2	−0.199	−29.20
8	2232	−4758	6990	−58.6	−0.469	−65.92
Inner Shaft						
1	887	−3434	4321	−30.6	−0.258	−85.06
3	3373	−8070	11443	−53.3	−0.418	−92.47
4	624	−2726	3350	−40.7	−0.229	−37.73
5	1547	−4325	5872	28.5	−0.358	−47.06
6	1208	−5299	6507	−47	−0.228	−19.14
7	2155	−9049	11204	−35.7	−0.238	−29.20
8	4035	−9785	13820	−60.6	−0.412	−65.92
Outer Shaft						
1	6278	−2091	8362	29.9	−3.002	−85.06
3	7400	−3381	10781	37.6	−2.189	−92.47
4	2804	−1268	4072	51.7	−2.211	−37.73
5	5315	−1796	7111	−44.3	−2.959	−47.06
6	8617	−2459	11076	56.2	−3.504	−19.14
7	9043	−855	9898	37.1	−10.577	−29.20
8	16076	−5839	21915	21.9	−2.753	−65.92

Discussion

The load conditions applied generally produced similar results in terms of fracture location, as the sternal portion of the midshaft presented as the site of failure in each specimen. The overall failure to predict the exact location of fracture is not particularly surprising given the simplifying assumptions of structural and tissue homogeneity that were used to formulate theoretical predictions. Empirically speaking, however, it appears reasonable to conclude that despite idiosyncratic variation in the sample, similar load conditions can be expected to entail comparable fracture locations in "typical" ribs (i.e., ribs 4–9).

Predicting the mode of fracture is more problematic, as the sample was characterized by transverse, spiral, butterfly, and buckle fractures. Among the transverse category, both complete and incomplete fractures were observed. Under the intended loading condition (longitudinal bending in the rib's plane of curvature), conventional wisdom holds that—given bone's relative weakness in tension—fracture would commence along the tensile surface (in this case, the outer or parietal rib face). In the case of the incomplete transverse fractures this is clearly what happened, and we may infer this to have occurred in the complete transverse fractures as well. In two of the specimens with incomplete transverse fractures, the fracture lines terminated on the visceral rib face traveling in a more oblique direction, possibly indicating incipient failure along lines of shear. Butterfly fractures represent failure in bending that initiates in tension and as the original compressive surface is encountered, the fracture surface splits and follows planes of shear (5). In the present study, the single butterfly fracture observed presented on the parietal face; i.e., the putative tensile surface. What this probably represents is an unintentionally complex loading situation where the bending moment was not directed purely perpendicular to the visceral and parietal rib faces, but eccentric to them. The observation of a spiral fracture may represent yet another source of load encountered. Spiral fractures are typically associated with twisting (torsional) loads, in which the lines of tension on bone surfaces follows a sigmoid pattern at roughly 45° to the bone long axis. The spiral fracture represents failure along these tension lines. It is quite possible that end-loading a rib can impose torsion in addition to bending, if the curvature of the specimen is such that the plane of curvature of the specimen is not

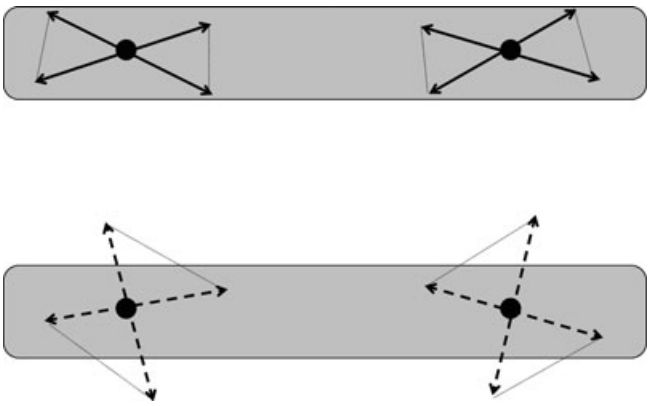

FIG. 3—*Schematic depiction of principal strain orientation and its variation across experiments. Sternal is to the left, vertebral end is to the right. Solid arrows represent principal strain direction on the outer (parietal) rib surface; dashed arrows represent principal strain direction on the inner (visceral) rib surface (as viewed from the parietal perspective). Arrows represent extrema of principal strain orientation; dotted lines joining arrowheads define the included range of variation. As depiction of local curvature is not provided, the perspective at each strain gage site should be interpreted as tangent to the bone surface at that location. Under the intended bending load in experiments, the expected orientation of maximum principal strain is longitudinal (i.e., parallel to the rib long axis) on the outer surface, and perpendicular to the rib long axis on the inner surface. Departures from this expected pattern can be attributed to (i) superimposition of twisting loads on the bending loads, and/or (ii) anisotropic material properties of the bone (i.e., analogous to the concept of "grain" in wood), which can cause principal stress and strain directions to diverge.*

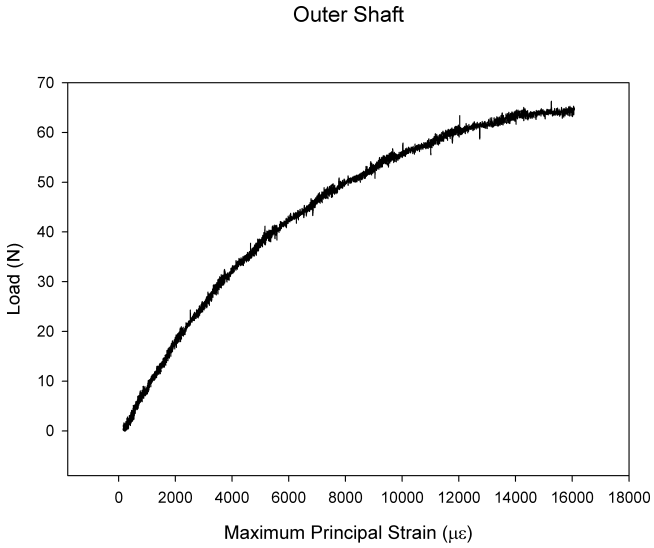

FIG. 4—*The relationship of load magnitude to tensile strain magnitude on the sternal shaft of specimen no. 8. The disproportionate increase in strain with load is indicative of plastic deformation of the specimen prior to failure. This interpretation is also supported by the measurement of strains in excess of 16,000 με at the time of failure, as this figure is over 50% greater than estimates of yield strain in cortical bone. Such high strains in sternal regions compared to those observed in the vicinity of the rib angle indicate greater energy absorption capacity in the bone tissue in the sternal shaft.*

coincident with the applied load. The evidence for this can be assessed with reference to the direction of maximum principal strain recorded during experiments (Fig. 3). If the desired effect of bending is accomplished, these directions ought to be aligned longitudinally on parietal surfaces and transversely along visceral surfaces. Principal strain directions that are obliquely disposed with respect to the specimen long axis (and orthogonal to one another between parietal and visceral faces) are likely indicative of some degree of torsional superimposition as well. By and large, the principal strain directions conform to the expectation that the ribs were primarily bent, rather than twisted, during experiments. Specifically, there is no evidence that the specimen exhibiting the spiral fracture was twisted any more or less than other individuals.

If, in fact, the desired control of load conditions was achieved in these experiments, the question arises as to why such an array of fracture patterns was observed. The obvious culprit is specimen variation, but whether subtle differences in specimen geometry, bone density and stiffness are implicated is difficult to tease apart. The gradual imposition of load on the specimens has no doubt influenced the results, as a high-impact version of these same experiments could be expected to produce comminuted fractures (5). What was established in these experiments was that the incomplete fractures produced *in vivo* (1,2) could be reproduced *in vitro*. The observation of both complete and incomplete fractures among our sample indicates that rib elements can fail in brittle or ductile fashion, which points to significant differences in stiffness and toughness among specimens. This intrinsic variation will complicate efforts to effectively relate fracture patterns to specific traumatic events.

The single case of a buckle fracture deserves further comment, if for no other reason than forensic anthropologists have inquired as to its etiology given the compressive strength that characterizes bone tissue, and because this type of fracture has been observed in samples subjected to blunt trauma (1,2). The buckle fracture is characterized as a localized failure in compression, often (as in our observed case) without any visible cracks. Buckling is expected in cases where a load is imposed on a very thin-walled structure and any local weakness precipitates failure. Although the material from which the structure is made is not irrelevant, buckling is primarily a structural issue of specimen geometry (3).

This observation alone is sufficient to question the validity of the stress analysis approach used here (referred to as *beam theory*, the analysis of structures under bending), as such an analysis implicitly assumes that buckling is not among the failure possibilities for the problem involved. The stress analysis also assumes elastic behavior; that is, stress and strain remain linearly related throughout an experiment, and that plastic (nonrecoverable) deformation is not occurring. Yet it is likely that significant plastic deformation preceded fracture in several experiments. For example, maximum principal strain in specimen 8 was 16,000 με at the outer shaft prior to failure. Given yield strain of around 9000 με for bone of various stiffness values, this specimen had become structurally compromised well before fracture was observed (Fig. 4). This observation is problematic from an analytical standpoint as proportional relationships between stress and strain can no longer be assumed.

Of particular interest are the strain magnitudes recorded at the gages closest to failure sites (outer surface of the shaft), which were of comparable distance to the fracture sites across experiments. An over 5-fold difference in principal and shear strains is observed at outer shaft gage sites across these experiments at the moment of failure. While this does not necessarily indicate equivalent difference in strain at the fracture site, it nevertheless suggests substantial differences in specimen stiffness, toughness, and probably strength (Table 2, Fig. 5). If this sample mirrors population variation even approximately, it suggests that behavior of ribs will be difficult to summarize via general biomechanical models. One of several possible culprits for the disparate results is the effects of age—an

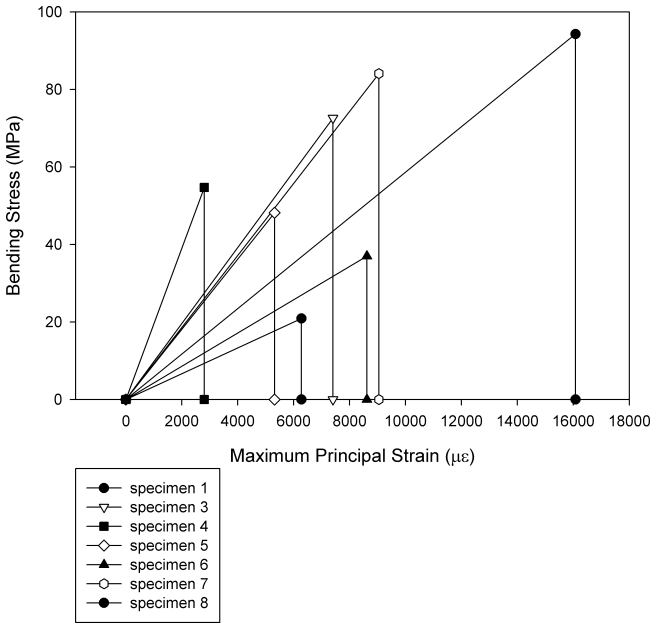

FIG. 5—*Hypothesized stress-strain curves of the outer rib shaft in seven experiments. The strain at failure is plotted against the hypothesized stress using the common flexural formula. The slopes of the lines from the beginning of experiments (stress and strain both zero) until the failure point provides a stiffness estimate in each specimen. The area enclosed by each triangle is proportional to the strain energy stored prior to failure. The differences observed cannot be ascribed to differences in specimen size; the stresses are normalized loads and the strains are proportional and not absolute deformations. The graph assumes perfectly elastic behavior of the ribs under load; however, we observed departures from a linear stress-strain relationship in several instances.*

uncontrolled variable in this study—which could have contributed to large individual differences in porosity and mineralization. Individual differences in brittleness may result.

A further indication that the theoretical modeling approach is inadequate concerns the disparity of stress estimates for the actual fracture sites (Table 2). If bone tissue is similar from rib to rib, we should be seeing values broadly congruent with one another. The calculated failure stress ranges from 33 to 150 MPa, which indicates these theoretical values are not very reliable. Estimates for the breaking stress of cortical bone vary depending on the loading context and the bone element, but in bending a failure stress of 200 MPa is reasonable (5). What is apparently a consistent underestimation of failure stress stems from at least two factors: (i) our use of rehydrated dry specimens (9) and (ii) our simplifying assumption that treats the ribs as solid sections of elliptical geometry. While incorporation of cortical thickness into an ellipse model would bring predicted stresses closer to the 200 MPa target, we would still observe an unacceptably large range of estimates across experiments. Changes in bone stiffness and shaft size and shape along the rib shaft violate the assumptions of homogeneity and prismatic structure to the point that the calculated stresses are not congruent with actual stresses created during experiments.

Thus, there is inconsistency in both the theoretical stresses and the observed strains at the time of structural failure, but because stress is a unit load and strain is a proportional measure of deformation, the expectation is that measures of both should be fairly similar from specimen to specimen. Several variables contribute to this departure from expectation, but the fact that the ribs yielded prior to macroscopic fracture suggests that our assumption of elastic behavior in calculating stress is simply invalid in this case. Explaining the large discrepancies in strains measured at failure is more challenging, but the assumption that breaking strains should be comparable among the sample is premised on the ribs being free of local defects, and such unseen points of weakness may dictate—to some unknown degree—both the mode and precise location of fracture.

Of course, more sophisticated models can be developed for estimating stress and strength of ribs (17), but these are time- and resource-intensive and require precise measurement of both material and structural properties. Such an approach is impractical and even undesirable when the purpose of the model is to be able to generalize about the context of fracture based on a few easily measured variables. For this reason, our view is that application of experimental, rather than computational or theoretical, approaches be utilized for associating rib fractures with specific physical events. Thus, while the recommendation of Love and Symes (2) that structural and material criteria are important in understanding fracture in forensic contexts is sound, it is important to recognize that advances in bone fracture mechanics are currently driven by experimental data (18,19).

The strain data from our experiments suggest that the mechanical properties of rib bone are regionally variable. Specifically, it would appear that the anterior rib shaft is more compliant than the posterior shaft in the vicinity of the angle. This is no doubt due in part to the low stiffness of the anterior rib cross-sections under the load examined, but Cormier's experimental data also indicate that the bone tissue itself here is relatively compliant, and weaker (13). There is an advantage conferred by this compliance, however, in that the anterior rib shaft is probably capable of more energy absorption prior to failure (Fig. 5, the area under the stress–strain curve is proportional to toughness at a given location). This might explain observations related to dynamic impacts, where the "strong" areas of the rib can fracture while the weaker anterior shaft remains intact (2).

In the case of the clinical observation of "flail chest," traumatic thoracic compression produces fractures at both the angle and sternal shaft in individual ribs. This observation prompts a necessary caveat that the mechanical environment of single bone failure may differ substantially from bone behavior *in vivo*. Eventually, inferences drawn from the data of this and other (1,2) studies should be tested in intact cadavers in which *in vivo* conditions of trauma can be more closely approximated. This will be particularly important for understanding the etiology of brittle (complete) versus ductile (incomplete) rib fracture. The degree to which mechanical testing of individual rib elements can be extrapolated to understanding *in vivo* failure of ribs—where the thorax is behaving as a composite structure—remains an open question. Our experiments were, however, able to replicate fracture patterns that are recovered from forensic contexts. These experiments also suggest that similar loading events can produce consistent locations of bone failure even though the mode of fracture is variable.

Conclusion

In vitro tests of human ribs were conducted to evaluate whether rib fracture patterns would be consistent under controlled loading conditions, despite idiosyncratic variation in rib morphology. While the site of fracture was fairly consistent throughout experiments, the mode of fracture was remarkably variable. A simple beam model to calculate site of fracture based on stress magnitude appears to be unsuitable for both empirical and theoretical reasons. Validation of models of rib fracture will require a large experimental foundation.

Human ribs may undergo considerable plastic deformation prior to complete structural failure. Our experiments indirectly support

previous data (13) that the anterior rib shafts are less stiff and less strong than the posterior regions of the same element. Because the reduced stiffness probably enhances energy absorption capacity in the anterior shaft, rib fractures can potentially occur in regions that are comparatively "strong" by standard biomechanical measures.

References

1. Love JC, Symes SA, Ferraro C. Understanding rib fracture patterns. Proceedings of the 55th Annual Meeting of the American Academy of Forensic Sciences, Chicago, IL, 2003 Feb 17–22; Colorado Springs, CO: American Academy of Forensic Science, 2003;257–8.
2. Love JC, Symes SA. Understanding rib fracture patterns: incomplete and buckle fractures. J Forensic Sci 2004;49:1153–8.
3. Vogel S. Life's devices: the physical world of animals and plants. Princeton, NJ: Princeton University Press, 1988.
4. Turner CH, Burr DB. Basic biomechanical measurements of bone: a tutorial. Bone 1993;14:595–608.
5. Martin RB, Burr DB, Sharkey NA. Skeletal tissue mechanics. New York: Springer, 1998.
6. White TD. Human osteology. San Diego: Academic, 1991.
7. Evans FG. Mechanical properties of bone. Springfield, IL: Charles C Thomas, 1973.
8. Broz JJ, Simske SJ, Greenberg AR, Luttges MW. Effect of rehydration state on the flexural properties of whole mouse bones. J Biomech Eng 1993;115:447–9.
9. Currey JD. The effects of drying and re-wetting on some mechanical properties of cortical bone. J Biomech 1988;21:439–41.
10. Martin RB, Sharkey NA. Mechanical effects of postmortem changes, preservation, and allograft bone treatments. In: Cowin SC, editor. Bone mechanics handbook. Boca Raton: CRC Press, 2001;20-1–20-24.
11. Turner CH, Burr DB. Experimental techniques for bone mechanics. In: Cowin SC, editor. Bone mechanics handbook. Boca Raton: CRC Press, 2001;7-1–7-35.
12. Young WC. Roark's formulas for stress and strain. New York: McGraw Hill, 1989.
13. Cormier JM. Microstructural and mechanical properties of human ribs [MS Thesis]. Blacksburg, VA: Virginia Polytechnic Institute and State University, 2003.
14. Keyak JH, Rossi SA. Prediction of femoral fracture load using finite element models: an examination of stress- and strain-based failure theories. J Biomech 2000;33:209–14.
15. Wang S-J, Wei HW, Chen CS. Comments on prediction of femoral fracture load using automated finite element modeling: by J. H. Keyak et al. J Biomech 2001;34:559–60.
16. Ruff CB, Runestad JA. Primate limb bone structural adaptations. Annu Rev Anthropol 1992;21:407–33.
17. Niu Y, Shen W, Stuhmiller JH. Finite element models of rib as an inhomogeneous beam structure under high-speed impacts. Med Eng Physics 2007;29:788–98.
18. Nalla RK, Stolken JS, Kinney JH, Ritchie RO. Fracture in human cortical bone: local fracture criteria and toughening mechanisms. J Biomech 2005;38:1517–25.
19. Peterlik H, Roschger P, Klaushofer K, Fratzl P. From brittle to ductile fracture of bone. Nat Mater 2006;5:52–5.

Additional information and reprint requests:
David J. Daegling, Ph.D.
Department of Anthropology
University of Florida
1112 Turlington Hall
Gainesville, FL 32611-7305
E-mail: daegling@anthro.ufl.edu